Analytical Biochemistry 642 (2022) 114563

Contents lists available at ScienceDirect

Analytical Biochemistry

journal homepage: www.elsevier.com/locate/yabio

Designing a novel DNA-based electrochemical biosensor to determine of Ba^{2+} ions both selectively and sensitively

Nastaran Ebrahimi, Jahan Bakhsh Raoof *, Reza Ojani, Maryam Ebrahimi

Electroanalytical Chemistry Research Laboratory, Department of Analytical Chemistry, Faculty of Chemistry, University of Mazandaran, Babolsar, Iran

ARTICLE INFO

Keywords:
Ba^{2+} ions
DNA-Based biosensor
Carmoisine
Modified carbon paste electrode

ABSTRACT

This work describes a novel electrochemical biosensor based on G-quadruplex (G4) DNA for the sensitive and selective detection of Ba^{2+} ions using a Carbon Paste Electrode modified with Ag nanoparticles incorporated in reduced Graphene Oxide via a simple wet chemical method (Ag-rGO/CPE), in the presence of carmoisine (CA) as a new electrochemical indicator. The peak current of CA increased with increasing Ba^{2+} ions concentration and the DNA-based sensor showed linear ranges of 0.06–0.80 nM and 1.0–80 nM and a Limit of Detection (LOD) of 0.045 nM. The proposed biosensor showed a good selectivity toward Ba^{2+} ions in the presence of other metal ions such as Ag^{+}, Hg^{2+}, K^{+} and Na^{+} and was applied to the analysis of natural samples showing appropriate results.

1. Introduction

Consuming products that contain Ba^{2+} ions may cause some problems to human health such as hypopotassaemia, gastroenteritis, changes in nerve reflexes, muscle weakness and cardiac arrhythmias [1–3]. The number of Ba^{2+} ions in drinking water and food is low, but its application in medicine as radiographic agent and as semiconductors production in electronic industry has increased in recent years [4–6]. Therefore, because of the pollution growth as a result of these activities, it is necessary to develop sensitive and selective techniques to detect and quantify Ba^{2+} ions.

Although there are different methods reported for analytical determination of Ba^{2+} ions such as atomic absorption spectroscopy [7], ICP-coupled mass spectroscopy [8,9], flow injection analysis and flame atomic emission spectrometry [10], fluorescence spectroscopy [11] and electrochemical methods [12–17], it seems that the electrochemical methods are more suitable for this purpose due to good properties such as high selectivity and sensitivity, being less time consuming and inexpensive.

Recently, nanomaterials have been used for modification of electrodes with the purpose of improving some properties of the electrochemical sensors such as selectivity and sensitivity [18–20]. High electrical conductivity, large surface area and good mechanical strength of graphene-based materials have led to their application in various fields such as DNA-based sensors [21–23], energy storage device [24,25], solar cells [26], antibiotics removal in water treatment [27], analytical extraction processes [28] and peptide cleavage-based biosensor [29]. Ag nanoparticles have been applied in different chemical reactions because of good catalytic properties and electron transport ability [30–32]. Therefore, Ag nanoparticles incorporated in rGO have been used to develop an electrochemical DNA-based sensor in this work.

Carmoisine (CA) is a food dye with different names like Brilliant carmoisine O, azorubin S and acid Red 14 [33]. It is an anionic dye with azo dye group (Scheme 1) that can interacts with the DNA structure. Dehghan et al. carried out a study in which they investigated the interactive behavior of CA with native calf thymus DNA via applying spectroscopic and electrochemical methods [34]. Several compounds such as methylene blue and ethyl green have been used as electroactive labels [35,36]. It is worth mentioning that CA, which interacts with DNA, can give a strong reduction peak current due to reduction of azo function. To the best of our knowledge, no DNA-based sensors have been developed to detect Ba^{2+} ions using CA as a label.

G-quadruplex (G4) is a nucleic acid with non-canonical structure formed by bending guanine-rich sequences of DNA or RNA. G4 DNA has drawn great attention because of its ability to be used in both signal transduction and target recognition [37]. Due to G4 DNA ability to bind with some metal ions, it can be used for construction of DNA-based biosensor [38,39]. A wide range of electrochemical biosensors has been developed because of their easy modification, cost-effectiveness and chemical stability [37,40–42].

In this work, CA was applied as a new electroactive label for the electrochemical detection of Ba^{2+} ions using a DNA-based sensor. CPEs

* Corresponding author.
E-mail address: j.raoof@umz.ac.ir (J.B. Raoof).

https://doi.org/10.1016/j.ab.2022.114563
Received 11 September 2021; Received in revised form 16 January 2022; Accepted 17 January 2022
Available online 29 January 2022

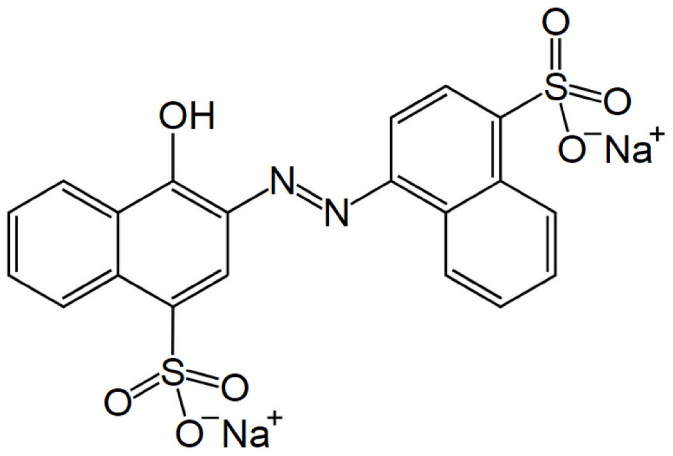

Scheme 1. The chemical structure of CA.

were modified with Ag-rGO to improve the electrochemical behavior of the biosensor. The performance of the biosensor has been evaluated, as well as its applicability to the analysis of natural samples.

2. Experimental

2.1. Chemicals and reagents

The oligonucleotide (5′-GGGT GGGT GGGT GGGT-3′) was purchased from BIONEER (South Korea) as the DNA probe. Potassium chloride, sodium chloride, barium nitrate, silver nitrate, potassium permanganate, sulfuric acid, hydrochloric acid, N, N-Dimethylformamide (DMF) and mercury nitrate were supplied from Merck chemical company. Potassium ferricyanide and potassium ferrocyanide were purchased from Fluka Company. CA, graphite powder and Polyvinylpyrrolidone (PVP K30) were purchased from Sigma-Aldrich. All reagents were used without purification.

Stock solution of DNA (1.0 μM) was prepared in Tris buffer solution (50 mM Tris-HCl, 1.0 mM EDTA, pH 8.0). To prepare double-stranded DNA (ds-DNA), equal amounts of ss-DNA and its complementary DNA were mixed. The solution was heated in water batch at 100 °C for 15 min and cooled in room temperature. Stock solutions of metal ions and CA with concentration of 1.0 mM were prepared in 50.0 mM Tris–HCl buffer (pH 7.4). Distilled, deionized and sterilized water was used to prepare aqueous solutions.

2.2. Instrumentation

Field Emission Scanning Electron Microscopy (FE-SEM) images and Energy-Dispersive X-ray Spectroscopy (EDS) results were recorded using a Mira 3-XMU instrument. All of the electrochemical analyses such as Differential Pulse Voltammetry (DPV), Electrochemical Impedance Spectroscopy (EIS) and Cyclic Voltammetry (CV) were done using an Autolab PGSTAT 30 potentiostat galvanostat (EcoChemie, The Netherlands), GPES 4.9 software package and FRA software (Eco Chemie, The Netherlands). Double beams UV spectrophotometer (CECIL 5000, elegant technology) computation was used to record UV–Vis absorption spectra.

2.3. Ag-rGO preparation

Graphene Oxide (GO) was prepared through improved Hummers' method [43]. Briefly, 1.0 g of graphite flake was added to a mixture of H_2SO_4/H_3PO_4 (120:13.5 mL) and then 6.0 g of $KMnO_4$ was slowly added in ambient temperature. The reaction content was heated at 50 °C for 12 h at stirring condition. When the reaction mixture cooled, it was poured into the mixture of ice (200 mL) and H_2O_2 (3 mL). Solid material was separated by the centrifuge and then washed with 70 mL of water, 70 mL of 30% HCl and 70 mL of ethanol (× 2). Finally, the obtained solid was dried in vacuum oven for 24 h in room temperature. Ag-rGO was prepared in the following steps [44]: 35 mg of the prepared GO was added to a beaker which contained 70 mL of DMF and sonicated for 1 h, 70 mL of DMF, 3.5 mmol of $AgNO_3$ and 0.7 g of PVP were added in another beaker respectively too. The solution was stirred for 1 h. Finally, two mixtures were put in a round-bottom flask and heated at 90 °C for 20 h to form Ag-rGO. The solid product was separated via the centrifuge and then washed with 20 mL of water and 30 mL of ethanol, respectively and dried in the oven for 24 h at 40 °C.

2.4. Ag-rGO/CPE preparation

0.5 g of graphite powder, proper amount of paraffin oil and 3% (w/w) Ag-rGO were thoroughly mixed in a mortar until a uniform paste is formed in order to prepare Ag-rGO/CPE. The prepared paste was filled into 4.0 mm diameter glass tube. A Cu wire was inserted from the other side of glass tube to make electrical contact.

2.5. Immobilization of ss-DNA on Ag-rGO/CPE

The Ag-rGO/CPE was immersed in a solution of 0.50 M acetate buffer solution (pH 4.8) and 20 mM of NaCl and then the potential of 1.8 V vs. SCE was applied on the surface of Ag-rGO/CPE for 5 min without being stirred to immobilize ss-DNA on Ag-rGO/CPE. After washing the surface of electrode with deionized water, it was immersed in 50.0 mM of Tris-HCl buffer solution (pH = 7.4) containing 10^{-6} M of DNA in stirring condition and the potential of 0.5 V vs. SCE was applied through chronoamperometry method for the immobilization of ss-DNA at the surface of Ag-rGO/CPE.

2.6. G4 DNA formation and accumulation of CA on the biosensor

After immobilization of ss-DNA on the surface of modified electrode, G4 DNA formation was done by immersing ss-DNA/Ag-rGO/CPE for 5 min in buffer solution (0.05 M Tris–HCl buffer solution, pH = 7.4) which contained different concentrations of Ba^{2+} ions in stirring condition. In addition, potential was not applied to the biosensor at this step. Then the surface of the biosensor was washed with sterilized and deionized water to remove unbounded metal ions. In order to accumulate CA on G4 DNA/Ag-rGO/CPE, the biosensor was immersed in 1.0 mM of CA solution (50 mM Tris–HCl buffer solution, pH = 7.4) for 5 min and finally the surface of the electrode was rinsed with sterilized and deionized water.

3. Results and discussion

3.1. Characterization of Ag-rGO

FE-SEM was applied to investigate surface morphology of the prepared Ag-rGO. Also, EDS measurement was used for elemental composition analysis. According to results in Fig. 1a, carbon, oxygen and silver atoms are present in the prepared nano-composite with 61.73, 20.90 and 17.37 percentages, respectively. As it can be seen in Fig. 1b, the prepared GO had sheets with thickness of about 46 nm. The results which are shown in Fig. 1c and (d), reveal that Ag nanoparticles were uniformly constructed with good population on rGO surface. Average diameter of 68.4 nm was calculated for Ag nanoparticles. The efficiency of modified electrode increased owing to the electrocatalytic effect of Ag-rGO.

3.2. Electrochemical characterization of the modified electrodes

Materials such as Ag nanoparticles and rGO can change the conductivity and rate of electron transfer on the surface of electrode. CV and EIS are useful techniques to investigate the resistance changes on the

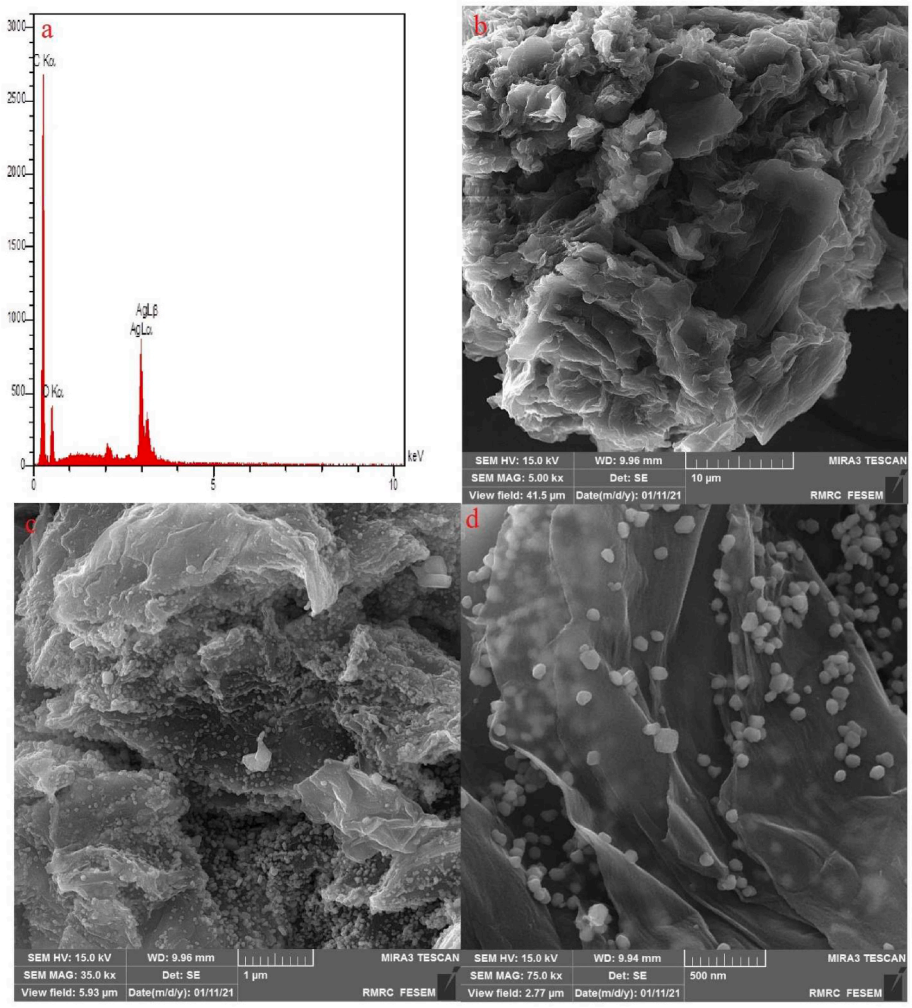

Fig. 1. EDS spectrum analysis of Ag-rGO (a), FE-SEM image of the GO (b) and FE-SEM images of the Ag-rGO nanocomposite (c and d).

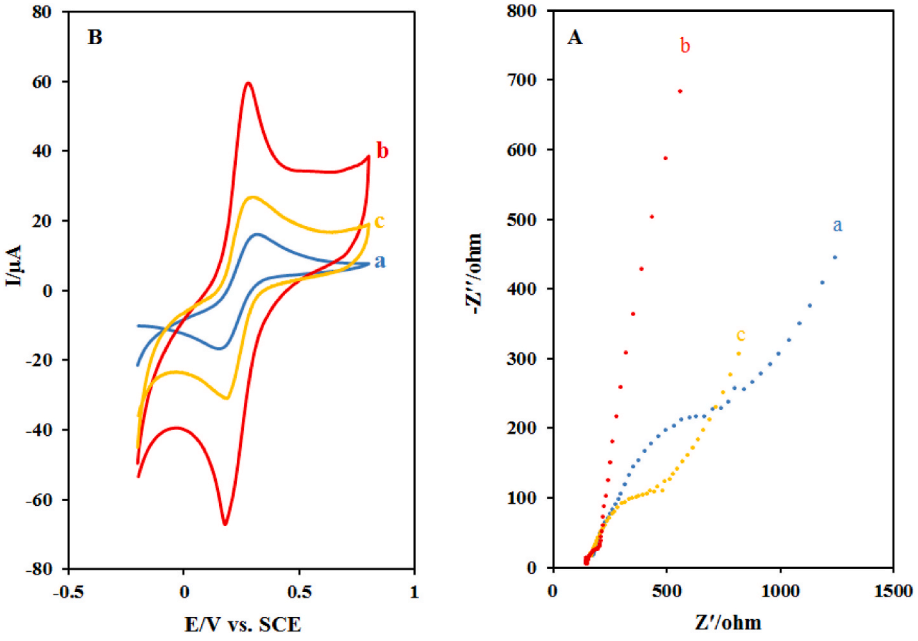

Fig. 2. Nyquist plots (A) and CV curves (B) of 1.0 mM $K_3[Fe(CN)_6]$/1.0 mM $K_4[Fe(CN)_6]$ in 10 mM Tris-HCl buffer solution (pH 7.0) at (a) bare CPE, (b) Ag-rGO/CPE and (c) G4/Ag-rGO/CPE after incubation in 10^{-3} M of Ba^{2+} ions at scan rate of 100 mV s^{-1}.

surface of electrode due to the presence of nano materials before and after modification. According to the published literature, the performance of electrochemical sensors is related to the electron or charge-transfer resistance (R_{et} or R_{ct}) [45,46]. The Nyquist plots (-z″ vs. z′) of (a) CPE, (b) Ag-rGO/CPE and (c) G4/Ag-rGO/CPE were recorded in a solution containing 1.0 mM of both $K_3[Fe(CN)_6]$ and $K_4[Fe(CN)_6]$ redox couple (Fig. 2A) to investigate the R_{ct} change at the surface of modified and unmodified electrodes. It can be observed that R_{ct} (semicircle diameter of Nyquist plots) of the Ag-rGO/CPE and G4/Ag- rGO/CPE decreased in comparison to that of CPE due to electrocatalytic effect of Ag-rGO nano composite. Moreover, the electron transfer resistance of G4/Ag-rGO/CPE is more than that of Ag-rGO/CPE which can be resulted from G4 construction ability to decrease the conductivity of the electrode surface. Also, Ag-rGO nano composite with good electrical conductivity can act as an interconnected conductive network, which can improve the performance of the modified electrode (biosensor).

In addition, voltammetric peak currents of $[Fe(CN)_6]^{3-/4-}$ redox couple were recorded at the surface of (a) CPE, (b) Ag-rGO/CPE and (c) G4/Ag-rGO/CPE (Fig. 2B). The peak currents of $[Fe(CN)_6]^{3-/4-}$ redox couple at surface of Ag-rGO/CPE and G4/Ag-rGO/CPE increased and it proves that using Ag-rGO to modify CPE can reduce electron transfer resistance on the surface of the G4/Ag-rGO/CPE.

3.2. Interaction between CA and G4

UV–Vis spectroscopy is a useful method to find three noncovalent modes (electrostatic, intercalation and groove binding) of small molecules with DNA [47–50]. Electrostatic binding between CA and our probe doesn't occur due to anionic structure of CA (Scheme 1). Therefore, intercalation and groove binding were investigated via UV–Vis spectroscopy method. UV–vis spectra of CA (curve a), CA-ss-DNA (curve b), CA-ds-DNA (curve c) and CA-G4 were recorded (Fig. 3) for this purpose. According to the previous reports [36,38,39], absorbance shift (red shift) and absorbance decrease (hypochromic effect) can be seen as a result of intercalating binding of small molecule with DNA. The magnitudes of hypochromic and red shifts are 10% and 1.1 nm for CA-ss-DNA, 13%, and 2.1 nm for CA-ds-DNA, 14% and 3.8 nm for CA-G4-DNA in the presence of 10^{-6} M Ba^{2+} ions, 16% and 4.4 nm in the presence of 10^{-5} M Ba^{2+} ions (Fig. 3). These results are lower than those observed for typical classical intercalator [51,52]. Therefore, the interaction between CA and G4-DNA is partly intercalation and domain interaction is groove binding. Furthermore, Dehghan et al. showed that CA can interacts with DNA in a groove-binding mode [34]. The interaction between CA and G4 (Fig. 4) was also investigated using DPV of CA before (curve a) and after adding various amounts of G4 (curves b–e). As it can be seen, the electrochemical signal of free CA decreased with the increase in the amount of G4 due to the accumulation of Ba^{2+} ions concentration. In addition, positive peak potential shifts of CA were observed with the increase of Ba^{2+} ions concentrations. According to the electrochemical investigation of interaction between DNA and small molecules [47,48] and report by Bard et al. [53], positive peak potential shift in voltammetric study can confirm the intercalation interaction.

3.4. Circular dichroism (CD) investigation of Ba^{2+} ions-inducted G-quadruplex formation

CD spectroscopy can be used as a suitable method to investigate proteins and nucleic acids structures. CD spectroscopy studies are based on this fact that materials with left- and right-hands orientation have differences in absorbance of the circularly-polarized light [54,55]. G-quadruplexes have two parallel and antiparallel-stranded structure types based on the orientation [56–59]. CD spectroscopy was used to distinguish the structure type of G4 in the current study. CD spectrum of G4 with parallel-stranded structure has a maximum at ~260 nm and a minimum at ~240 nm; on the other hand, G4 with antiparallel-stranded structure has a maximum at ~290 nm and a minimum at ~260 nm [56]. Therefore, and as Fig. 5 shows the probe was formed with parallel-stranded structure in the presence of Ba^{2+} ions (Curve a). Curve b shows CD spectrum of the G4 that was formed in the presence of Ba^{2+} ions and CA. As a result, the presence of CA cannot influence the G4 formation. In addition, the heights of maximum and minimum peaks of CD spectrum were increased after 5-min interaction between Ba^{2+} ions and DNA probe (curve c).

3.5. Electrochemical determination of Ba^{2+} ions at the surface of G4/Ag-rGO/CPE

The sensitivity of new biosensor was investigated at the optimum conditions and the results were shown in Fig. 6. For this purpose, ss-DNA/Ag-rGO/CPE was incubated in different concentrations of Ba^{2+} ions solutions and then DPV method was used for recording differential pulse voltammograms of 10^{-3} M CA that was intercalated with G4. The electrochemical reduction peak current of CA increased following the increase in Ba^{2+} ions concentration due to ss-DNA structural switch to Ba^{2+}-stabilized G4. Because of this phenomenon, the accumulation of CA at the surface of G4/Ag-rGO/CPE increased with the increase of

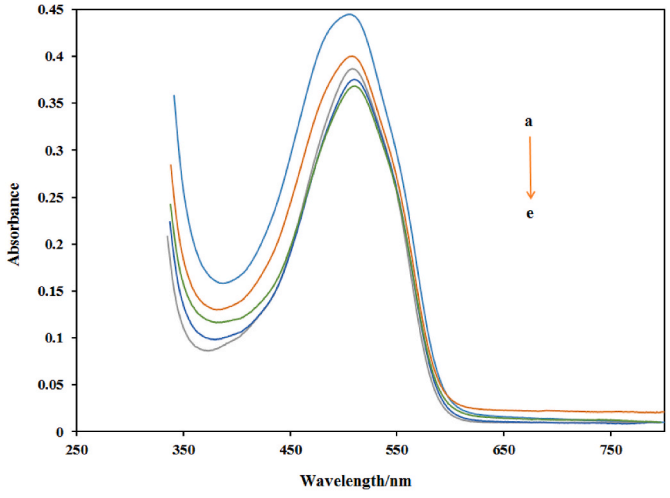

Fig. 3. The UV–Vis spectra of 10^{-5} M CA (curve a), ss-DNA- CA (curve b), ds-DNA- CA (curve c), G4 probe - CA in the presence of 10^{-6} M (curve d) and 10^{-5} M (curve e) of Ba^{2+} ions in aqueous solutions.

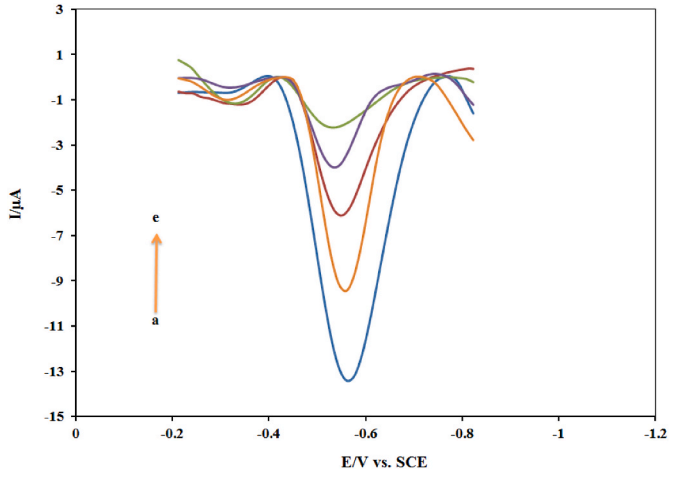

Fig. 4. Differential pulse voltammograms of 10^{-5} M CA in solution before (curve a) and after adding probe in the presence of various concentrations of Ba^{2+}: 10^{-6} M (curve b), 10^{-5} M (curve c), 10^{-4} M (curve d) and 10^{-3} M (curve e) at Ag-rGO/CPE.

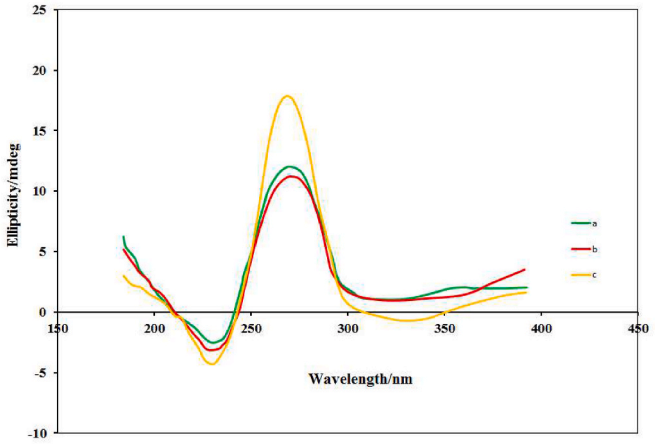

Fig. 5. CD spectra of Ba^{2+} ions-probe (a), Ba^{2+} ions-probe in the presence of CA (b) and Ba^{2+} ions-probe after 5 min of intercalation (c).

different Ba^{2+} ions concentrations and then the reduction peak current of CA increased (Fig. 6A). Fig. 6B shows two linear relationships between peak currents of CA before and after its intercalation with the G4 (ΔI) and Ba^{2+} ions concentration at the ranges of 0.06–0.8 nM and 1.0–80 nM. The calculated LOD was 0.045 nM (S/N = 3). The electrochemical parameters in determining Ba^{2+} ions were compared with the other reports and the results were listed in Table 1. It can be seen that the present method can provide high sensitivity, wide linear range and comparable detection limit.

3.6. Selectivity investigation of the biosensor in the electro-detection of Ba^{2+} ions

The sequence of DNA is important in forming G4. There are different algorithmic rules to predict which sequence of DNA can form G4 [60,61]. The thermal stability of G4 is dependent on the concentration of monovalent cations, especially in case of K^+ and Na^+ [62]. Some G4s are unstable to be formed even at 5 °C and some G4s are stable above 95 °C [63]. Therefore, the formation of stable G4 depends on sequence of DNA and concentration of cations [62]. According to these reasons, the selectivity of designed biosensor was studied by investigating the effect of several ions such as Ag^+, Hg^{2+}, K^+ and Na^+ on DNA probe structural switch from ss-DNA to G4 (stabilized with ions). Fig. 7 shows DPV response of 10^{-3} M-accumulated CA on the surface of G4/Ag-rGO/CPE, which is incubated in Ba^{2+} ions (curve f) and the mentioned ions (curves b-e). As it can be seen, the DPV cathodic peak currents of CA have no significant change before incubation (curve a) and after it in Ag^+, Hg^{2+}, K^+ and Na^+ solution with constant concentration (curves b-e). This result proved that the proposed biosensor has good selectivity and can be used to determine Ba^{2+} ions electrochemically.

3.7. Electrochemical sensing of Ba^{2+} ions in real sample at G4/Ag-rGO/CPE

The applicability of the biosensor for electrochemical detection of Ba^{2+} ions was investigated in sea and tap water as real samples. Different concentrations of Ba^{2+} ions were spiked in real samples and standard addition method was used to determine Ba^{2+} ions electrochemically via the proposed method. Table 2 summarizes the results of this study. It is clear that there is a very good agreement between spiked values and founded values and it confirms the applicability of G4/Ag-

Table 1
Comparison of the various electrochemical sensors for determination of Ba^{2+} ions.

Analyte	Electrode	LDR (μM)	LOD (μM)	Ref.
Ba^{2+}	PVC-based neutral carrier and organic exchanger membranes	14–100000	–	[12]
	PVC membrane sensor	50–100000	2.5	[64]
	Electrolytic cell with four electrode	10–500	–	[65]
	barium (II) PVC membrane sensor	1–10000	0.56	[66]
	G4/Ag-rGO/CPE	0.00006-0.0008 0.001-0.08	0.000045	present study

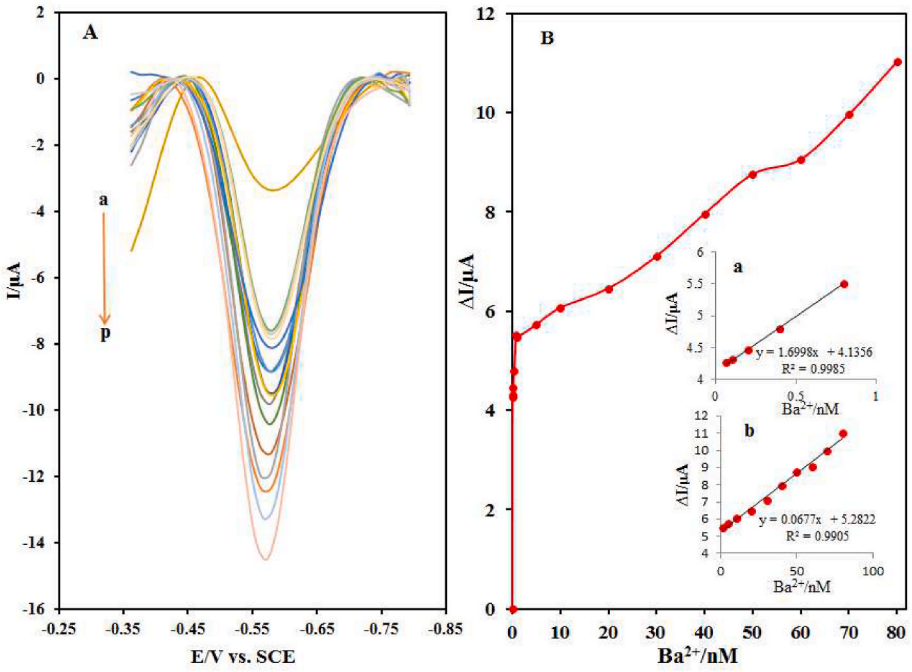

Fig. 6. A) DPV curves of 10^{-3} M-accumulated CA on the G4/Ag-rGO/CPE in 50 mM Tris–HCl buffer solution (pH = 7.4) containing various concentrations of Ba^{2+}ions: (a) 0.0, (b) 0.06, (c) 0.1, (d) 0.2, (e) 0.4, (f) 0.6, (g) 0.8, (h) 1.0, (i) 5.0, (j) 10.0, (k) 20.0, (l) 30.0, (m) 40.0, (n) 50.0, (o) 60.0 and (p) 80.0 nM. (B) The difference of cathodic peaks current in the absence and presence of Ba^{2+} ions (ΔI) in the differential pulse voltammograms (A) against the Ba^{2+} ions concentrations. Inset shows the related calibration plots of Ba^{2+} ions concentrations in the ranges (a) 0.06–0.8 nM and (b) 1–80 nM.

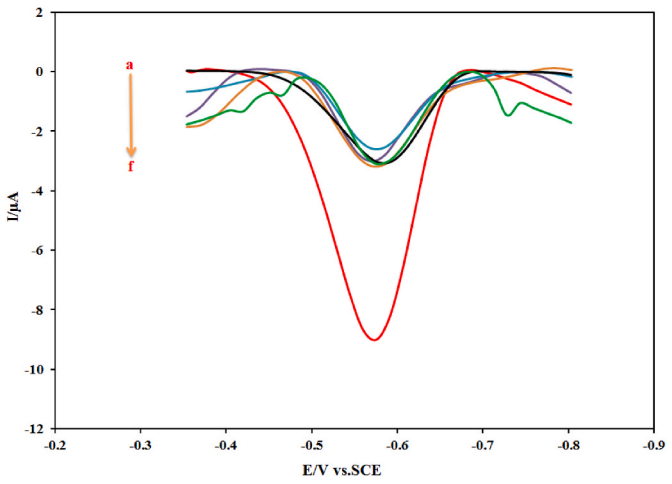

Fig. 7. DPV responses of 10^{-3} M-accumulated CA on the G4/Ag-rGO/CPE (a) before and after incubation in 1.0 μM (b) Ag^{+}, (c) Hg^{2+}, (d) Na^{+}, (e) K^{+} and 1.0 nM (f) Ba^{2+} ions at the surface of G4/Ag-rGO/CPE.

Table 2
The ability of proposed method for electrochemical analysis of Ba^{2+} ions in water samples as real samples.

Water sample	Ba^{2+} added/M	Ba^{2+} found/M[a]	Recovery (%)
Tap water [b]	0	No detectable	–
	1.0×10^{-9}	$1.07(\pm0.03) \times 10^{-9}$	107.0
	30.0×10^{-9}	$30.3(\pm0.05) \times 10^{-9}$	100.1
Sea water [c]	0	Not detectable	–
	1.0×10^{-9}	$0.92(\pm0.01) \times 10^{-9}$	92.0
	30.0×10^{-9}	$29.6(\pm0.06) \times 10^{-9}$	98.6

[a] Mean value ± SD (standard deviation), n = 3.
[b] From drinking water system of Babolsar, Iran.
[c] From Caspian Sea, Babolsar, Iran.

rGO/CPE for the electrochemical detection of Ba^{2+} ions in real samples.

3.8. Stability and reproducibility of G4/Ag-rGO/CPE

The stability and reproducibility of the proposed biosensor were also evaluated. For this purpose, six individual G4/Ag-rGO/CPEs were prepared and DPV method was used to record the reduction of CA peak currents in the constant concentration of Ba^{2+} ions and the relative standard deviation (RSD %) was calculated 5.3%. In addition, stability of the biosensor was investigated by DPV responses of CA at the surface of G4/Ag-rGO/CPE before and after storing it for 2 weeks at 4 °C. The response retained 91.23% in comparison with the initial signal. According to the results, the biosensor showed good stability and reproducibility.

4. Conclusion

An electrochemical DNA-based sensor was constructed using Ag-rGO/CPE to detect Ba^{2+} ions in the presence of CA as a new electrochemical indicator. A wide detection range and a low LOD were achieved due to the fast electron transfer from the Ag-rGO nanocomposite. The distance between CA and the electrode surface is reduced in the formation of the G4 structure in the presence of Ba^{2+} ions and therefore, the peak current of CA increases. G4/Ag-rGO/CPE was applied to the electrochemical determination of Ba^{2+} ions in sea and tap water and good results were achieved. In addition, the biosensor showed appropriate reproducibility and stability.

CRediT authorship contribution statement

Nastaran Ebrahimi: Investigation, Writing – original draft, Resources. **Jahan Bakhsh Raoof:** Supervision, Conceptualization, Data curation, Writing – review & editing, Funding acquisition, Visualization. **Reza Ojani:** Methodology, Formal analysis, Visualization. **Maryam Ebrahimi:** Methodology, Formal analysis, Writing – review & editing, Visualization.

References

[1] H. Choudhury, R. Cary, W.H. Organization, Barium and Barium Compounds, World Health Organization, 2001, https://doi.org/10.1002/14356007.a03_325.pub2.
[2] F. Gingele, A. Dahmke, Discrete barite particles and barium as tracers of paleoproductivity in South Atlantic sediments, Paleoceanography 9 (1) (1994) 151–168, https://doi.org/10.1029/93PA02559.
[3] O. Celebi, A. Kilikli, H. Erten, Sorption of radioactive cesium and barium ions onto solid humic acid, J. Hazard Mater. 168 (2–3) (2009) 695–703, https://doi.org/10.1016/j.jhazmat.2009.02.090.
[4] S. Brooks, Pulmonary Reactions to Miscellaneous Mineral Dusts, Man-Made Mineral Fibers, and Miscellaneous Pneumoconioses, Occupational Respiratory Diseases, National Institute of Occupational Safety and Health, Washington, 1986, pp. 431–432.
[5] R. Kresse, U. Baudis, P. Jäger, H.H. Riechers, H. Wagner, J. Winkler, H.U. Wolf, Barium and Barium Compounds, Ullmann's Encyclopedia of Industrial Chemistry, 2000, https://doi.org/10.1002/14356007.a03_325.pub2.
[6] D. Moffett, C. Smith-Simon, Y.-W. Stevens, Toxicological profile for barium and barium compounds. https://www.atsdr.cdc.gov/toxprofiles/tp24.pdf, 2007.
[7] T. Atsdr, ATSDR (Agency for Toxic Substances and Disease Registry), Prepared by Clement International corp., under Contract, vol. 205, 2000, 88-0608.
[8] G. Komaromy-Hiller, K.O. Ash, R. Costa, K. Howerton, Comparison of representative ranges based on US patient population and literature reference intervals for urinary trace elements, Clin. Chim. Acta 296 (1–2) (2000) 71–90, https://doi.org/10.1016/S0009-8981(00)00205-9.
[9] I. Rosborg, B. Nihlgård, L. Gerhardsson, Hair element concentrations in females in one acid and one alkaline area in southern Sweden, AMBIO A J. Hum. Environ. 32 (7) (2003) 440–446.
[10] C. Plamboeck, H.C. Westtoft, S.A. Pedersen, J.E. Andersen, Filterless pre-concentration by co-precipitation by formation of crystalline precipitate in the analysis of barium by FIA-FAES, J. Anal. At. Spectrom. 18 (1) (2003) 49–53, https://doi.org/10.1039/B209984E.
[11] K. Chaichana, N. Phutlaprungrueang, L. Chaicharoenwimolkul, M. Promkatkaew, S. Kongsriprapan, A selective fluorescence probe based on naphthalene for the detection of barium (ii), Spectrochim. Acta Mol. Biomol. Spectrosc. 207 (2019) 118–122, https://doi.org/10.1016/j.saa.2018.09.006.
[12] V.K. Gupta, A.K. Jain, U. Khurana, L. Singh, PVC-based neutral carrier and organic exchanger membranes as sensors for the determination of Ba2+ and Sr2+, Sensor. Actuator. B Chem. 55 (2–3) (1999) 201–211, https://doi.org/10.1016/S0925-4005(99)00046-5.
[13] M.W. Laeubli, O. Dinten, E. Pretsch, W. Simon, F. Voegtle, F. Bongardt, T. Kleiner, Barium-selective electrodes based on neutral carriers and their use in the titration of sulfate in combustion products, Anal. Chem. 57 (14) (1985) 2756–2758, https://doi.org/10.1021/ac00291a005.
[14] U. Lal, M. Chattopadhyaya, A. Dey, Heterogeneous ion selective electrodes based on electroneutral ioncarriers: barium (II) and nickel (II) electrodes, J. Indian Chem. Soc. 59 (4) (1982) 493–496.
[15] G. Moody, J. Thomas, J. Lima, A. Machado, Characterisation of poly (vinyl chloride) barium ion-selective electrodes without an internal reference solution, Analyst 113 (7) (1988) 1023–1027, https://doi.org/10.1039/AN9881301023.
[16] C.A. Woolever, H.D. Dewald, Differential pulse anodic stripping voltammetry of barium and lead in gunshot residues, Forensic Sci. Int. 117 (3) (2001) 185–190, https://doi.org/10.1016/S0379-0738(00)00402-3.
[17] K. Suzuki, K. Tohda, H. Sasakura, T. Shirai, Barium ion selective electrode based on natural carboxylic polyether antibiotic salinomycin, Anal. Lett. 20 (1) (1987) 39–45, https://doi.org/10.1080/00032718708082235.
[18] K. Xu, J. Huang, Z. Ye, Y. Ying, Y. Li, Recent development of nano-materials used in DNA biosensors, Sensors 9 (7) (2009) 5534–5557, https://doi.org/10.3390/s90705534.
[19] S. He, B. Song, D. Li, C. Zhu, W. Qi, Y. Wen, L. Wang, S. Song, H. Fang, C. Fan, A graphene nanoprobe for rapid, sensitive, and multicolor fluorescent DNA analysis, Adv. Funct. Mater. 20 (3) (2010) 453–459, https://doi.org/10.1002/adfm.200901639.
[20] L. Li, Y. Wen, Q. Xu, L. Xu, D. Liu, G. Liu, Q. Huang, Application of carbon nanomaterials in gene delivery for endogenous RNA interference in vitro and in vivo, Curr. Pharmaceut. Des. 21 (22) (2015) 3191–3198.
[21] M. Pumera, Electrochemistry of graphene: new horizons for sensing and energy storage, Chem. Rec. 9 (4) (2009) 211–223, https://doi.org/10.1002/tcr.200900008.
[22] M. Pumera, A. Ambrosi, A. Bonanni, E.L.K. Chng, H.L. Poh, Graphene for electrochemical sensing and biosensing, TrAC Trends Anal. Chem. (Reference Ed.) 29 (9) (2010) 954–965, https://doi.org/10.1016/j.trac.2010.05.011.
[23] X. Cao, Ultra-sensitive electrochemical DNA biosensor based on signal amplification using gold nanoparticles modified with molybdenum disulfide,

graphene and horseradish peroxidase, Microchim. Acta 181 (9) (2014) 1133–1141, https://doi.org/10.1007/s00604-014-1301-y.
[24] M.D. Stoller, S. Park, Y. Zhu, J. An, R.S. Ruoff, Graphene-based ultracapacitors, Nano Lett. 8 (10) (2008) 3498–3502, https://doi.org/10.1021/nl802558y.
[25] R. Pal, S.L. Goyal, I. Rawal, A.K. Gupta, Ruchi, Efficient energy storage performance of electrochemical supercapacitors based on polyaniline/graphene nanocomposite electrodes, J. Phys. Chem. Solid. 154 (2021) 110057, https://doi.org/10.1016/j.jpcs.2021.110057.
[26] X. Wang, L. Zhi, K. Müllen, Transparent, conductive graphene electrodes for dye-sensitized solar cells, Nano Lett. 8 (1) (2008) 323–327, https://doi.org/10.1021/nl072838r.
[27] M.-f. Li, Y.-g. Liu, G.-m. Zeng, N. Liu, S.-b. Liu, Graphene and graphene-based nanocomposites used for antibiotics removal in water treatment: a review, Chemosphere 226 (2019) 360–380, https://doi.org/10.1016/j.chemosphere.2019.03.117.
[28] F. Pena-Pereira, V. Romero, I.d.l. Calle, I. Lavilla, C. Bendicho, Graphene-based nanocomposites in analytical extraction processes, TrAC Trends Anal. Chem. (Reference Ed.) (2021) 116303, https://doi.org/10.1016/j.trac.2021.116303.
[29] F. Meng, H. Sun, Y. Huang, Y. Tang, Q. Chen, P. Miao, Peptide cleavage-based electrochemical biosensor coupling graphene oxide and silver nanoparticles, Anal. Chim. Acta 1047 (2019) 45–51, https://doi.org/10.1016/j.aca.2018.09.053.
[30] B. Zheng, G. Liu, A. Yao, Y. Xiao, J. Du, Y. Guo, D. Xiao, Q. Hu, M.M. Choi, A sensitive AgNPs/CuO nanofibers non-enzymatic glucose sensor based on electrospinning technology, Sensor. Actuator. B Chem. 195 (2014) 431–438, https://doi.org/10.1016/j.snb.2014.01.046.
[31] H. Li, C.-Y. Guo, C.-L. Xu, A highly sensitive non-enzymatic glucose sensor based on bimetallic Cu–Ag superstructures, Biosens. Bioelectron. 63 (2015) 339–346, https://doi.org/10.1016/j.bios.2014.07.061.
[32] C. Qi, J. Zheng, Novel nonenzymatic hydrogen peroxide sensor based on Ag/Cu2O nanocomposites, Electroanalysis 28 (3) (2016) 477–483, https://doi.org/10.1002/elan.201500296.
[33] K. Amin, H.A. Hameid II, A. Abd Elsttar, Effect of food azo dyes tartrazine and carmoisine on biochemical parameters related to renal, hepatic function and oxidative stress biomarkers in young male rats, Food Chem. Toxicol. 48 (10) (2010) 2994–2999, https://doi.org/10.1016/j.fct.2010.07.039.
[34] M. Arvin, G. Dehghan, M.A. Hosseinpourfeizi, A.A. Moosavi-Movahedi, Spectroscopic and electrochemical studies on the interaction of carmoisine food additive with native calf thymus DNA, Spectrosc. Lett. 46 (4) (2013) 250–256, https://doi.org/10.1080/00387010.2012.723663.
[35] F. Li, J. Peng, Q. Zheng, X. Guo, H. Tang, S. Yao, Carbon nanotube-polyamidoamine dendrimer hybrid-modified electrodes for highly sensitive electrochemical detection of microRNA24, Anal. Chem. 87 (9) (2015) 4806–4813.
[36] M. Ebrahimi, J.B. Raoof, R. Ojani, Novel electrochemical DNA hybridization biosensors for selective determination of silver ions, Talanta 144 (2015) 619–626, https://doi.org/10.1016/j.talanta.2015.07.020.
[37] H. Yang, Y. Zhou, J. Liu, G-quadruplex DNA for construction of biosensors, TrAC Trends Anal. Chem. (Reference Ed.) (2020) 116060, https://doi.org/10.1016/j.trac.2020.116060.
[38] M. Ebrahimi, J.B. Raoof, R. Ojani, Design of a novel electrochemical biosensor based on intramolecular G-quadruplex DNA for selective determination of lead (II) ions, Anal. Bioanal. Chem. 409 (20) (2017) 4729–4739, https://doi.org/10.1007/s00216-017-0416-5.
[39] N. Ebrahimi, J.B. Raoof, R. Ojani, M. Ebrahimi, A novel G-quadruplex DNA-based biosensor for sensitive electrochemical determination of thallium (I) ions, J. Iran. Chem. Soc. 18 (2) (2021) 407–413, https://doi.org/10.1007/s13738-020-02035-5.
[40] P. Zhu, S. Li, S. Zhou, N. Ren, S. Ge, Y. Zhang, Y. Wang, J. Yu, In situ grown COFs on 3D strutted graphene aerogel for electrochemical detection of NO released from living cells, Chem. Eng. J. 420 (2021) 127559, https://doi.org/10.1016/j.cej.2020.127559.
[41] X. Liu, X. Gao, L. Yang, Y. Zhao, F. Li, Metal–Organic framework-functionalized paper-based electrochemical biosensor for ultrasensitive exosome assay, Anal. Chem. 93 (34) (2021) 11792–11799, https://doi.org/10.1021/acs.analchem.1c02286.
[42] Y. Zhang, J. Xu, S. Zhou, L. Zhu, X. Lv, J. Zhang, L. Zhang, P. Zhu, J. Yu, DNAzyme-triggered visual and ratiometric electrochemiluminescence dual-readout assay for Pb(II) based on an assembled paper device, Anal. Chem. 92 (5) (2020) 3874–3881, https://doi.org/10.1021/acs.analchem.9b05343.
[43] D.C. Marcano, D.V. Kosynkin, J.M. Berlin, A. Sinitskii, Z. Sun, A. Slesarev, L. B. Alemany, W. Lu, J.M. Tour, Improved synthesis of graphene oxide, ACS Nano 4 (8) (2010) 4806–4814, https://doi.org/10.1021/nn1006368.
[44] S. Dutta, C. Ray, S. Sarkar, M. Pradhan, Y. Negishi, T. Pal, Silver nanoparticle decorated reduced graphene oxide (rGO) nanosheet: a platform for SERS based low-level detection of uranyl ion, ACS Appl. Mater. Interfaces 5 (17) (2013) 8724–8732, https://doi.org/10.1021/am4025017.
[45] L. Wang, T. Meng, D. Zhao, H. Jia, S. An, X. Yang, H. Wang, Y. Zhang, An enzyme-free electrochemical biosensor based on well monodisperse Au nanorods for ultra-sensitive detection of telomerase activity, Biosens. Bioelectron. 148 (2020) 111834, https://doi.org/10.1016/j.bios.2019.111834.
[46] H. Zhao, Y. Chang, R. Liu, B. Li, F. Li, F. Zhang, M. Shi, L. Zhou, X. Li, Facile synthesis of Vulcan XC-72 nanoparticles-decorated halloysite nanotubes for the highly sensitive electrochemical determination of niclosamide, Food Chem. 343 (2021) 128484, https://doi.org/10.1016/j.foodchem.2020.128484.
[47] J. Chen, J. Zhang, Q. Zhuang, J. Chen, X. Lin, Electrochemical studies of the interaction of 2-nitroacridone with DNA and determination of DNA, Electroynalysis (N.Y.N.Y.) 19 (17) (2007) 1765–1772, https://doi.org/10.1002/elan.200703929.
[48] Q. Wang, X. Wang, Z. Yu, X. Yuan, K. Jiao, Spectroscopic and electrochemical studies on the binding mechanism of DNA with an anthraquinone biological dye, nuclear fast red, Int. J. Electrochem. Sci. 6 (2011) 5470–5481. http://electrochemsci.org/papers/vol6/6115470.pdf.
[49] Q.-X. Wang, K. Jiao, F.-Q. Liu, X.-L. Yuan, W. Sun, Spectroscopic, viscositic and electrochemical studies of DNA interaction with a novel mixed-ligand complex of nickel (II) that incorporates 1-methylimidazole and thiocyanate groups, J. Biochem. Biophys. Methods 70 (3) (2007) 427–433, https://doi.org/10.1016/j.jbbm.2006.09.011.
[50] S. Khan, S.A. Nami, K. Siddiqi, E. Husain, I. Naseem, Synthesis and characterization of transition metal 2, 6-pyridinedicarboxylic acid derivatives, interactions of Cu (II) and Ni (II) complexes with DNA in vitro, Spectrochim. Acta Mol. Biomol. Spectrosc. 72 (2) (2009) 421–428, https://doi.org/10.1016/j.saa.2008.10.001.
[51] S. Ramakrishnan, M. Palaniandavar, Mixed-ligand copper (II) complexes of dipicolylamine and 1, 10-phenanthrolines: the role of diimines in the interaction of the complexes with DNA, J. Chem. Sci. 117 (2) (2005) 179–186, https://doi.org/10.1007/BF03356114.
[52] Q. Wang, W. Li, F. Gao, S. Li, J. Ni, Z. Zheng, Comprehensive studies on the DNA-binding and cleavage properties of a nickel complex derived from phthalate and 1, 10-phenanthroline, Polyhedron 29 (1) (2010) 539–543, https://doi.org/10.1016/j.poly.2009.06.066.
[53] M.T. Carter, M. Rodriguez, A.J. Bard, Voltammetric studies of the interaction of metal chelates with DNA. 2. Tris-chelated complexes of cobalt (III) and iron (II) with 1, 10-phenanthroline and 2, 2'-bipyridine, J. Am. Chem. Soc. 111 (24) (1989) 8901–8911, https://doi.org/10.1021/ja00206a020.
[54] G.R. Bishop, J.B. Chaires, Characterization of DNA structures by circular dichroism, Curr. Protoc. Nucleic Acid Chem. 11 (1) (2002), https://doi.org/10.1002/0471142700.nc0711s11, 7.11. 1-7.11. 8.
[55] H. Porumb, M. Monnot, S. Fermandjian, Circular dichroism signatures of features simultaneously present in structured guanine-rich oligonucleotides: a combined spectroscopic and electrophoretic approach, Electrophoresis 23 (7-8) (2002) 1013–1020, https://doi.org/10.1002/1522-2683(200204)23:7/8<1013::AID-ELPS1013>3.0.CO;2-B.
[56] S. Burge, G.N. Parkinson, P. Hazel, A.K. Todd, S. Neidle, Quadruplex DNA: sequence, topology and structure, Nucleic Acids Res. 34 (19) (2006) 5402–5415, https://doi.org/10.1093/nar/gkl655.
[57] B. Ruttkay-Nedecky, J. Kudr, L. Nejdl, D. Maskova, R. Kizek, V. Adam, G-quadruplexes as sensing probes, Molecules 18 (12) (2013) 14760–14779, https://doi.org/10.3390/molecules181214760.
[58] A.-M. Chiorcea-Paquim, A.M. Oliveira-Brett, Redox behaviour of G-quadruplexes, Electrochim. Acta 126 (2014) 162–170, https://doi.org/10.1016/j.electacta.2013.07.150.
[59] Z. Bagheryan, J.B. Raoof, R. Ojani, E. Hamidi-Asl, Introduction of Ketamine as a G-quadruplex-binding ligand using platinum nanoparticle modified carbon paste electrode, Electroanalysis 25 (12) (2013) 2659–2667, https://doi.org/10.1002/elan.201300418.
[60] J. Huppert, Hunting G-quadruplexes, Biochimie 90 (8) (2008) 1140–1148.
[61] A.K. Todd, Bioinformatics approaches to quadruplex sequence location, Methods 43 (4) (2007) 246–251.
[62] H.M. Wong, O. Stegle, S. Rodgers, J.L. Huppert, A toolbox for predicting g-quadruplex formation and stability, J. Nucleic Acids 2010 (2010).
[63] P. Hazel, J. Huppert, S. Balasubramanian, S. Neidle, Loop-length-dependent folding of G-quadruplexes, J. Am. Chem. Soc. 126 (50) (2004) 16405–16415.
[64] A.M. Othman, M.S. El-Shahawi, M. Abdel-Azeem, A novel barium polymeric membrane sensor for selective determination of barium and sulphate ions based on the complex ion associate barium(II)–Rose Bengal as neutral ionophore, Anal. Chim. Acta 555 (2) (2006) 322–328, https://doi.org/10.1016/j.aca.2005.09.016.
[65] Z. Sun, E. Wang, A new electrochemical method based on transfer at a liquid/liquid interface: determination of barium and strontium, Talanta 35 (9) (1988) 673–677, https://doi.org/10.1016/0039-9140(88)80159-0.
[66] H.A. Zamani, M.T. Hamed-Mosavian, E. Aminzadeh, M.R. Ganjali, M. Ghaemy, H. Behmadi, F. Faridbod, Construction of barium (II) PVC membrane electrochemical sensor based on 3-deoxy-d-erythro-hexos-2-ulose bis (thiosemicarbazone) as a novel ionophore, Desalination 250 (1) (2010) 56–61, https://doi.org/10.1016/j.desal.2009.09.014.